Oxygen Isotopic Fractionation in Clouds: A Bin-Resolved Microphysics Model Approach

Thibault Hiron, Andrea Flossmann

JGR Atmospheres

RESEARCH ARTICLE
10.1029/2019JD031753

Oxygen Isotopic Fractionation in Clouds: A Bin-Resolved Microphysics Model Approach

Thibault Hiron[1] **and Andrea I. Flossmann**[1]

[1]Université Clermont Auvergne/CNRS, Laboratoire de Météorologie Physique, Clermont-Ferrand, France

Key Points:
- A new isotopologue module was added to the bin-detailed model Descam for precise fractionation description
- The microphysical evolution of a convective cloud impacts the isotopic ratio in the precipitation
- The size of the hydrometeors and the temperature, relative humidity, and isotopic ratio at the ground are of critical importance

Correspondence to:
T. Hiron,
thibault.hiron@opgc.univ-bpclermont.fr

Citation:
Hiron, T., & Flossmann, A. I. (2020). Oxygen isotopic fractionation in clouds: A bin-resolved microphysics model approach. *Journal of Geographical Research: Atmospheres*, *125*, e2019JD031753. https://doi.org/10.1029/2019JD031753

Received 10 OCT 2019
Accepted 25 SEP 2020
Accepted article online 27 SEP 2020

Abstract Measurements of the ratio of oxygen-18 to oxygen-16 are often used to reconstruct past climate or to quantify phase changes. However, in most models, the evolution of the isotopic ratio is calculated using the Rayleigh parameterization. The Descam model has recently been extended to simulate isotopic fractionation from occurring condensation/evaporation processes and the mass of oxygen-18 in aerosol particles, droplets, and ice crystals explicitly as a function of their size. In a first step, isotopic calculations are implemented into the 1.5D dynamical framework where several sensitivity studies are conducted to test the evolution of the isotopic ratio as a function of the different phase changes in a convective cloud. Though an isotopic signature can be identified for different microphysical pathways, the predominant factor for the isotopic ratio in the precipitation seems to be the dynamical evolution of the considered cloud.

1. Introduction

The stable oxygen isotopes of H_2O are essential for the study of past climates. They make up only a small part of all water molecules, but during phase changes, they behave differently due to differences in saturation vapor pressure and molecular diffusivity. Molecules containing heavier isotopes condense more easily, and their preference for the condensed phase is exacerbated by colder temperatures, so that in past colder precipitation events, their abundance is used as a proxy for assessing past climates ("isotopic thermometer"). Indeed, this feature has been used extensively for reconstructing past temperatures (e.g., Hays & Grossman, 1991).

Equally, modeling of the isotopic fraction of water vapor and condensed water has been done for the simulation of past climates or other large-scale phenomena (e.g., Joussaume & Jouzel, 1993)

Even though a number of exciting and convincing results were derived from these studies, the modification of the water isotopologues (water molecules containing an oxygen or hydrogen isotope) by clouds is a lot more complex than usually considered. Precipitation on snow packs is generally preceded by water cycling though several cloud events, and the occurring phase changes are heavily influenced by the clouds and the hydrometeors they are composed of. In particular, the size of the drops and ice crystals plays a role in the fractionation, that is, the modification of the isotopic ratio. An open remaining question is if these repeated fractionations can create such large modifications that they mask the global temperature signature or at least bias it.

The current study is a first bin-detailed attempt to shed light on the influence of small-scale cloud effects on the overall fractionation of water isotopologues. The detailed scavenging model (DESCAM; Flossmann & Wobrock, 2010), coupled to the simplified dynamics of a 1.5D convective cloud, allows one to follow in detail the evolution of drop and ice particles inside the cloud and in the forming precipitation. This microphysics module has been extended to include the treatment of water isotopologues. A number of sensitivity studies are performed to study the influence of the initial isotopic concentration, the microphysics of the cloud, and its dynamics. As the occurring phase transitions change the isotopic ratio in the condensed water, it is studied below if an observation of the isotopic ratio in the rain water will allow insights on the microphysics of the cloud (ice or liquid water) and the pathway of precipitation formation. Furthermore, the influence of the exact calculation of the fractionation is investigated.

2. Desription of the Model and Its Initial Conditions

2.1. The Original DESCAM Model

DESCAM (Flossmann & Wobrock, 2010; Flossmann et al., 1985) is a size-resolved cloud microphysics module—coupled here with a 1.5D dynamics model (Asai & Kasahara, 1967; Leroy et al., 2006)—which follows explicitly the populations of aerosol particles on which water vapor condenses to form cloud droplets and ice crystals. All considered hydrometeor categories are distributed on a 39-bin logarithmically spaced mass histogram, and each size class at a grid point is followed separately during the evolution of the cloud. The equivalent radii range from 1 nm to 7 μm for the aerosol particles and 1 μm to 7 mm for the liquid cloud and rain droplets. The bins for the ice crystals are defined in order to have a mass equivalence between two corresponding grid categories of liquid droplets and ice crystals (Leroy et al., 2006).

DESCAM uses six different size distributions: number concentrations of aerosol particles [$\mathcal{N}_a(r_a)$], cloud droplets [$N_d(r_d)$], and ice crystals [$N_i(r_i)$] as well as the mass of particles in each of these categories ($\mathcal{M}_a(r_a)$ in the aerosol particles, $\mathcal{M}_d(r_d)$ in the cloud droplets, and $\mathcal{M}_i(r_i)$ in the ice crystals). The size distributions $\varphi(r)$ correspond to conservative variables and therefore follow a conservation equation:

$$\frac{\mathrm{d}\varphi(r)}{\mathrm{d}t} = \left.\frac{\mathrm{d}\varphi(r)}{\mathrm{d}t}\right|_{\mathrm{dyn}} + \left.\frac{\mathrm{d}\varphi(r)}{\mathrm{d}t}\right|_{\mathrm{mic}}. \tag{1}$$

The microphysical evolution of the different size distributions follows the following equations:

$$\left.\frac{\partial \mathcal{N}_a(r_a)}{\partial t}\right|_{\mathrm{mic}} = \left.\frac{\partial \mathcal{N}_a(r_a)}{\partial t}\right|_{\mathrm{act/deact}} + \left.\frac{\partial \mathcal{N}_a(r_a)}{\partial t}\right|_{\mathrm{con/eva}} + \left.\frac{\partial \mathcal{N}_a(r_a)}{\partial t}\right|_{\mathrm{coll}} + \left.\frac{\partial \mathcal{N}_a(r_a)}{\partial t}\right|_{\mathrm{nucl}}, \tag{2}$$

$$\begin{aligned}\left.\frac{\partial N_d(r_d)}{\partial t}\right|_{\mathrm{mic}} = {} & \left.\frac{\partial N_d(r_d)}{\partial t}\right|_{\mathrm{act/deact}} + \left.\frac{\partial N_d(r_d)}{\partial t}\right|_{\mathrm{con/eva}} + \left.\frac{\partial N_d(r_d)}{\partial t}\right|_{\mathrm{coal}} + \left.\frac{\partial N_d(r_d)}{\partial t}\right|_{\mathrm{break}} \\ & + \left.\frac{\partial N_d(r_d)}{\partial t}\right|_{\mathrm{coll}} + \left.\frac{\partial N_d(r_d)}{\partial t}\right|_{\mathrm{nucl}} + \left.\frac{\partial N_d(r_d)}{\partial t}\right|_{\mathrm{rim}} + \left.\frac{\partial N_d(r_d)}{\partial t}\right|_{\mathrm{melt}},\end{aligned} \tag{3}$$

$$\left.\frac{\partial N_i(r_i)}{\partial t}\right|_{\mathrm{mic}} = \left.\frac{\partial N_i(r_i)}{\partial t}\right|_{\mathrm{dep/sub}} + \left.\frac{\partial N_i(r_i)}{\partial t}\right|_{\mathrm{nucl}} + \left.\frac{\partial N_i(r_i)}{\partial t}\right|_{\mathrm{rim}} + \left.\frac{\partial N_i(r_i)}{\partial t}\right|_{\mathrm{melt}}. \tag{4}$$

The different terms treat the different microphysical processes of the atmosphere: the activation and deactivation of cloud droplets ($|_{\mathrm{act/deact}}$), the condensation and evaporation of water vapor on the aerosol particles and droplets ($|_{\mathrm{con/eva}}$) and the deposition and sublimation on the ice crystals ($|_{\mathrm{dep/sub}}$), the ice nucleation ($|_{\mathrm{nucl}}$), the collection of aerosol particles by the droplets (impaction scavenging, $|_{\mathrm{coll}}$), the collision coalescence between droplets ($|_{\mathrm{coal}}$) and subsequent breakup of large droplets ($|_{\mathrm{break}}$), the collision between droplets and ice crystals and subsequent freezing ($|_{\mathrm{rim}}$), and the instantaneous melting of the ice crystals when crossing the melting level ($|_{\mathrm{melt}}$).

The mathematical treatment of the different microphysical terms is summarized in Flossmann and Wobrock (2010), and details on the ice nucleation mechanisms can be found in Hiron and Flossmann (2015). Heterogeneous nucleation is parameterized using a combination of the Meyers et al. (1992) and Bigg (1953) parameterizations. Though not discussed here, as they only have a minor impact on the cloud dynamics (Hiron & Flossmann, 2015), deposition nucleation and contact freezing are also taken into account in Case A (section 3.1), as they are included in the parameterization by Meyers et al. (1992). The homogeneous nucleation mechanism, parameterized based on Koop et al. (2000), is highly dependent on the volume of the droplets. As the aerosol particle distribution considered in this case study is of marine origin with a low total particle number (section 2.3), there are only a small number of droplets in the cloud (the concentration at an altitude of 3.5 km after 20 min of integration time is 31 cm^{-3}), and they therefore reach quite large sizes early in the cloud development. This results in a very efficient homogeneous nucleation of ice particles, starting at temperatures as warm as −28°C. As this temperature is much higher than the generally accepted temperature for homogeneous nucleation (−36°C, a compromise was found by setting a threshold above which homogeneous nucleation is not considered. The temperature of −32°C was chosen as the threshold based on the different cases presented in Herbert et al. (2015, Figure 2).

The dynamic equations are resolved in a 1.5D dynamical frame (Asai & Kasahara, 1967) using two concentric cylindrical air columns, the inside column corresponding to an updraft (cloud) region and the outside concentric annular column for the surrounding compensating downward motion (cloudless) region. The radius of the outer cylinder (36 km) is 10 times larger than the inner cylinder (3.6 km), which allows one to consider that the cloud development in the inner cylinder has a minimal impact on the environment, which can be treated as a constant reservoir with only the vertical velocity being updated during the simulation. In the inner cylinder, the model follows the vertical variations of thermodynamical parameters and wind speeds, as well as the transport of aerosol particles and hydrometeors, as detailed in Leroy et al. (2006). The two cylinders also exchange aerosol particles, and the horizontal exchange allows for detrainment of hydrometeors into the environment.

2.2. New Isotopologue Module

In this study, the evolution of water isotopologues in the condensed phase is introduced in DESCAM for the first time. The new module treats one of the main isotopologues of water: molecules composed with oxygen-18 (hereafter only referred to as ^{18}O).

Commonly, the amount of heavy water isotopologues is quantified using the following ratio:

$$\delta^{18}O = 1{,}000 \cdot \left[\frac{\left(\frac{^{18}O}{^{16}O}\right)_{sample}}{\left(\frac{^{18}O}{^{16}O}\right)_{standard}} - 1 \right] \tag{5}$$

The definition is given as a deviation "per mil" (‰, parts per thousand), from a well-defined standard in order to improve global intercomparison of isotopic measurements. The most widely used standard is the Vienna Standard Mean Ocean Water (VSMOW Gonfiantini R., 1978) and corresponds to an isotopic concentration of

$$\left(\frac{^{18}O}{^{16}O}\right)_{VSMOW} = 22.28 \cdot 10^{-4}. \tag{6}$$

The isotopic concentration in a sample corresponds to the ratio of the water isotopologue masses, with

$$R_{v,iso} = \frac{\rho_{v,iso}}{\rho_{v,w}} = \frac{q_{v,iso}}{q_{v,w}} \tag{7}$$

for the gas phase partitioning. "$_{iso}$" values pertain to the water isotopologue composed with an ^{18}O atom while "$_{w}$" values pertain to H_2O molecules, assimilated to the total values. ρ_v is the water vapor content in g cm^{-3}, and q_v is the specific humidity (mixing ratio in $g_{water\,vapor}\,g_{air}^{-1}$) with $\rho \cdot q_v = \rho_v$.

2.2.1. Treatment of the Liquid Phase

The isotopic ratio of the liquid phase is defined as $R_{l,iso} = m_{l,iso}/m_{l,w}$, where m_l corresponds to the water mass in a drop.

In a state of equilibrium between the drops and the environing air mass, the equilibrium fractionation factor (Majoube, 1971; Merlivat & Nief, 1967), that is, the ratio between the vapor and condensed isotopic ratios, is only a function of temperature, extrapolated in this paper below −15°C, expressed as

$$\alpha_{l,^{18}O,eq} = \frac{R_{l,^{18}O}}{R_{v,^{18}O}} = \exp\left(\frac{1{,}137}{T^2} - \frac{0.4156}{T} - 2.0667 \cdot 10^{-3}\right), \tag{8}$$

with T the temperature in Kelvin.

However, this equilibrium fractionation is only valid at the interface between the drop and the air mass and therefore does not take into account the isotopic gradient in the water vapor due to temperature differences between the environment and the surface of the water drop as well as differences in molecular diffusivity for heavy and light water isotopologues. For this purpose, we use the kinetic fractionation, as proposed by Jouzel and Merlivat (1984) and formalized by Bolot et al. (2013):

$$\alpha_{l,kin} = \frac{\alpha_{l,eq}}{1 + (\beta_l - 1) \cdot \left(1 - \left[S_l^{eff}\right]^{-1}\right)}, \tag{9}$$

with β_l and S_l^{eff} as defined in appendix B in Bolot et al. (2013).

In the model, the evolution of the distributions of the mass of heavy water isotopologues in the aerosol particles and drops is determined by equations similar to Equations 2 and 3. The vapor exchange terms ($|_{\mathrm{con/eva}}$) are amended to take fractionation into account.

The variation of the heavy isotopologue mass $m_{\mathrm{l,iso}}$ for a liquid drop can, by definition, be expressed as

$$\frac{\mathrm{d}m_{\mathrm{l,iso}}}{\mathrm{d}t} = \overbrace{R_{\mathrm{l,iso}} \cdot \frac{\mathrm{d}m_{\mathrm{l},w}}{\mathrm{d}t}}^{\mathrm{I}} + \overbrace{m_{\mathrm{l},w} \cdot \frac{\mathrm{d}R_{\mathrm{l,iso}}}{\mathrm{d}t}}^{\mathrm{II}}. \tag{10}$$

This equation contains two physical phenomena: (I) the first right-hand term corresponds to the condensation or evaporation of water at the surface of the droplet, which is in equilibrium with its direct environment, and (II) the second right-hand term corresponds to the relaxation of the isotopic ratio in the droplet toward equilibrium with the environmental water vapor isotopic ratio as is detailed by Bolot et al. (2013) in their appendix B.

This relaxation is introduced in their equation (B4), which can be rewritten, using their equations (B5) through (B7), as the following differential equation:

$$\frac{\mathrm{d}R_{\mathrm{l,iso}}}{\mathrm{d}t} = \frac{1}{\tau_{\mathrm{drop}}} \left(\alpha_{\mathrm{l,kin}} R^{(\infty)}_{\mathrm{v,iso}} - R^{(\mathrm{s})}_{\mathrm{l,iso}} \right), \tag{11}$$

where τ_{drop} is the characteristic relaxation time as introduced by Bolot et al. (2013, their equation B5) and explicited here in Equation 13. This Equation 11 can be integrated to obtain the time evolution of the isotopic ratio through relaxation.

Finally, the evolution of the heavy isotopologue water mass in the droplets through condensation or evaporation follows

$$m_{\mathrm{l,iso}}(t+\Delta t) = m_{\mathrm{l,iso}}(t) + \underbrace{R^{(\mathrm{s})}_{\mathrm{l,iso}}(t)\Delta m}_{\mathrm{I}} + \underbrace{m(t)\left(\alpha_{\mathrm{l,kin}} R^{(\infty)}_{\mathrm{v,iso}} - R^{(\mathrm{s})}_{\mathrm{l,iso}}(t) \right)\left(1 - \exp^{-\frac{\Delta t}{\tau_{\mathrm{drop}}}} \right)}_{\mathrm{II}}, \tag{12}$$

where

$$\tau_{\mathrm{drop}} = \frac{r_d^2}{3} \frac{\rho_{\mathrm{l}}}{\rho^{(\infty)}_{\mathrm{v}}} \frac{\alpha_{\mathrm{l,kin}}}{D_{\mathrm{v,iso}} f_{\mathrm{v,iso}}}, \tag{13}$$

where r_d is the droplet radius, $D_{\mathrm{v,iso}}$ the molecular diffusivity, and $f_{\mathrm{v,iso}}$ the diffusion coefficient of heavy isotopologues.

2.2.2. Treatment of the Ice Phase

Similarly to the liquid phase, the isotopic ratio of the ice phase is defined as $R_{\mathrm{i,iso}} = m_{\mathrm{i,iso}}/m_{\mathrm{i,w}}$, where m_{i} corresponds to the water mass in an ice particle.

The equilibrium fractionation factor is expressed as (Majoube, 1970)

$$\alpha_{\mathrm{i},^{18}\mathrm{O,eq}} = \frac{R_{\mathrm{i},^{18}\mathrm{O}}}{R_{\mathrm{v},^{18}\mathrm{O}}} = \exp\left(\frac{11.839}{T} - 2.8224 \cdot 10^{-2} \right), \tag{14}$$

and the kinetic fractionation factor is defined in the same fashion as for the liquid phase (Equation 9).

Ideally, a detailed representation of the ice crystals where the isotopic ratio of each shell of the ice crystal is stored would be the correct representation, but such an approach is too expensive even for our simulation. Therefore, in this study, we assume that the isotopic ratio in the ice crystal is homogeneous, neglecting the slow self-diffusion of water in the ice phase. As a consequence, in a first approximation, the relaxation phenomenon presented for the liquid phase is neglected for ice crystals. Finally, similar to numerous other studies (e.g., Bony et al., 2008; Moore et al., 2016), we assume that no fractionation takes place during sublimation of ice crystals.

In the model, the evolution of the distributions of the mass of heavy water isotopologues in the ice crystals is determined by equations similar to Equation 4. The vapor exchange term ($|_{\mathrm{dep/sub}}$) is amended to take fractionation, with the presented restrictions, into account.

The variation of a heavy isotopologues mass $m_{\mathrm{i,iso}}$ for an ice crystal is therefore expressed as

$$\frac{\mathrm{d}m_{\mathrm{i,iso}}}{\mathrm{d}t} = \begin{cases} \alpha_{\mathrm{i,kin}} \cdot R_{\mathrm{v,iso}}^{(\infty)} \cdot \frac{\mathrm{d}m}{\mathrm{d}t} & \text{if } \frac{\mathrm{d}m}{\mathrm{d}t} \geq 0 \\ R_{\mathrm{i,iso}} \cdot \frac{\mathrm{d}m}{\mathrm{d}t} & \text{else} \end{cases} \tag{15}$$

with $\alpha_{\mathrm{i,kin}}$ defined in the same manner as $\alpha_{\mathrm{l,kin}}$ in Equation 9.

2.3. Initial Conditions

The dynamical framework is initialized using the well-documented reference case of the Cooperative COnvective Precipitation Experiment (CCOPE) (Dye et al., 1986), a small thunderstorm observed on 19 July 1981 in Montana (USA). The thermodynamic parameters necessary for the dynamical initialization of the model (temperature, pressure, and humidity) are taken from vertical sounding profiles measured shortly before the beginning of the CCOPE storm. To force convection, a surface heating of 2.3°C is applied during the first 10 min of integration time (Leroy et al., 2006).

The dry aerosol particle size distribution is initialized using a superposition of three lognormal number distributions:

$$\mathcal{N}_a(r_a) = \sum_{i=1}^{3} \frac{n_i}{\sqrt{2\pi}\ln 10 \log \sigma_i} \exp\left(-\frac{\log^2(r_a/R_i)}{2\log^2\sigma_i}\right), \tag{16}$$

with R_i the mean particle radius (μm), n_i the integral of the ith lognormal function (cm^{-3}), and σ_i a measure of the spectrum width as proposed by Jaenicke (1988). For the parameters, the values for a maritime air mass are used: n_i = 133, 66.6, and 3.06; R_i = 0.0039, 0.133, and 0.29; and log σ_i = 0.657, 0.210, and 0.396. The aerosol particles are chemically assimilated to $(NH_4)_2SO_4$ with a κ value of 0.61 (Petters & Kreidenweis, 2007).

The vertical distribution of water isotopologues at the initialization of the model is based on a Rayleigh distillation profile (Dansgaard, 1964):

$$R_{v,\mathrm{iso}}(z) = R_{v,\mathrm{iso}}(z=0) \cdot \left(\frac{q_v(z)}{q_v(z=0)}\right)^{\alpha_{l,\mathrm{eq}}(z)-1} \tag{17}$$

and with ^{18}O set so that at ground level, the deuterium excess equals 10‰ with a calculated deuterium profile interecepting at low altitude with the Scottsbluff sounding from (Ehhalt, 1974) $\delta^{18}\mathrm{O}(z=0) = -16°$ and $\delta\mathrm{D}(z=0) = -117.4°$.

3. Model Results

This study uses the same sensitivity methodology as in Hiron and Flossmann (2015): based on the CCOPE dynamical intialization and using the maritime air mass aerosol size distribution, four simulations are performed. One with all ice nucleation mechanisms active (Case A, section 3.1), one with no ice nucleation mechanisms active (Case B, section 3.3.1), one with only homogeneous nucleation active (Case C, section 3.3.2), and one with only heterogeneous nucleation active (Case D, section 3.3.3).

3.1. Reference Case A: All Ice Nucleation Mechanisms

We consider reference Case A for isotopic fractionation where all microphysics processes are involved. The liquid water content (LWC in g m^{-3}) and ice water content (IWC in g m^{-3}) as a function of time (min) and altitude (km) are displayed in Figure 1, left. The initial levels for 0°C (later referred to as iso-zero level) and −32°C (later referred to as homogeneous nucleation line) are also represented in the graph to facilitate the analysis of the results. Due to deposition nucleation, an early cirrus-like cloud forms at high altitude early on in the simulation. This early formation does not impact the global dynamics of the system. The cloud starts forming around 3 km altitude after 8.5 min of integration time and quickly grows over 25 min to reach an altitude of 9.7 km. Ice nucleation starts around 5 km altitude, and the ice water content reaches 0.01 g m^{-3} for the first time as the cloud top reaches 6 km and the cloud then rapidly becomes glaciated. Precipitation is initiated mostly in the ice phase between 5.5 and 6.5 km after 30.5 min of integration time. It is accompanied by a decrease in the updraft velocity as part of the hydrometeors reaches a precipitating diameter. It is only later on, when the updraft has died down, that most of the condensed water mass precipitates.

The precipitation on the ground displays three distinctive regimes (black dashed curve in Figure 2, left): first a small peak of rainfall intensity which corresponds to the hydrometeors sedimenting from the precipitation

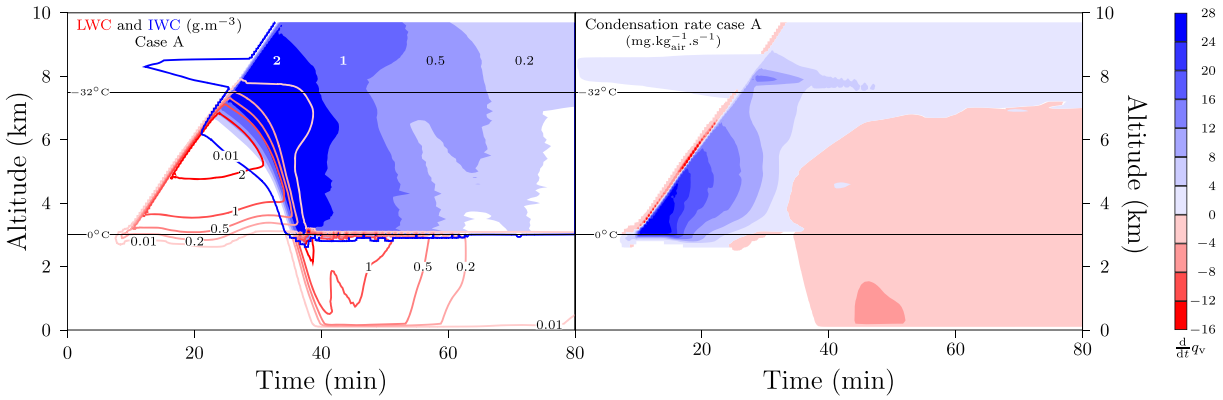

Figure 1. (Left) Liquid water content (g m^{-3}, red) and ice water content (g m^{-3}, blue) and (right) condensation rate (mg kg$^{-1}_{air}$ s^{-1}) as a function of altitude and time simulated for reference Case A with homogeneous and heterogeneous ice nucleation mechanisms active. The color scale pertains to the right panel.

onset associated with precipitating liquid water contents around 0.8 g m^{-3} and small downdrafts. Then, after 43 min of integration time, the rainfall intensity increases dramatically over a long period, though the liquid water content at the ground remains relatively constant. This evolution corresponds to a strong increase of the downdraft: the large precipitating ice water content reaching the iso-zero line leads to a large latent heat consumption during the melting of the ice crystals, which causes this strong downdraft. Finally, the downdraft dies down as the precipitating ice water content decreases, and the intensity of the precipitation weakens gradually. This results in a cumulative precipitation of 15.32 mm (Table 1).

The evolution of the isotopic ratio in the condensed phase as a function of altitude, and time is presented for the ^{18}O isotopologues in Figure 3, left. When the cloud starts forming after 8 min, a strong condensation rate is observed (larger than 25 mg kg$^{-1}_{air}$ s^{-1}; Figure 1, right) before gradually weakening as the cloud develops (the condensation rate has decreased to 9 mg kg$^{-1}_{air}$ s^{-1} when the cloud top reaches 7.5 km). In the updraft, we observe that the isotopic ratio decreases with increasing altitude and time, with $\delta^{18}O \sim -6°$ at the cloud base and $\delta^{18}O \sim -15°$ where the cloud reaches 7.5 km. A strong increase in the condensation in the cloud is observed between 7.5 and 8.5 km of altitude, corresponding to the contribution of homogeneous ice nucleation, as most of the remaining droplets freeze and the newly formed ice crystals draw more water vapor from the atmosphere. This however does not impact significantly the isotopic ratio in the condensed phase as the decrease of the isotopic ratio seems to occur at the same rate as earlier in the cloud development ($\delta^{18}O \sim -17°$ where the cloud reaches 9.7 km).

The early cirrus-like formation (between 7.7 and 8.5 km, until 25 min of integration time; Figure 3, left) displays a similar decrease of the isotopic ratio with altitude, but with much lower values ($\delta^{18}O_{cirrus}(25\text{ min}) \in [-46, -57]$, the shaded area corresponding to values out of the color scale, versus $\delta^{18}O_{main}(30\text{ min}) \in [-15, -16]$ for altitudes between 7.7 and 8.5 km). The early evolution of the isotopic ratio in the condensed phase inside of the cloud follows that of an air parcel: First, the fractionation in an atmospheric air parcel

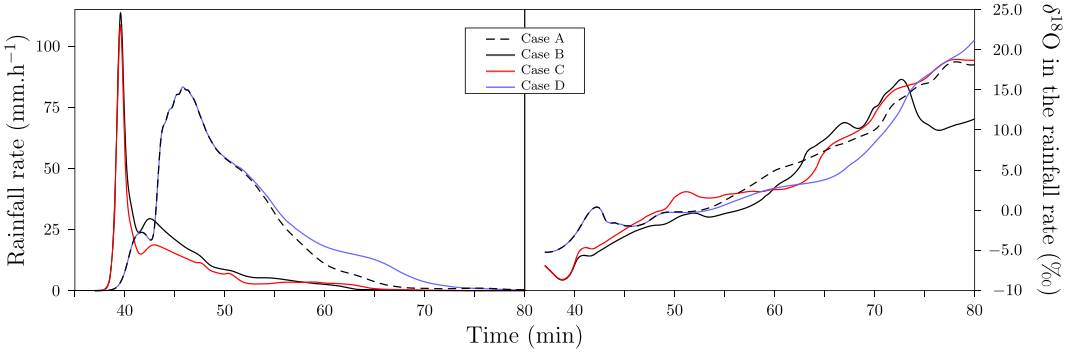

Figure 2. (left) Rainfall rate on the ground and (right) isotopic ratio in the instantaneous rainfall ($\delta^{18}O$, ‰) for all four cases (A in black dashed, B in black continuous, C in red, and D in blue).

Table 1
List of Case Studies With Their Ice Nucleation Processes and the Corresponding Results for the Cumulative Rain (mm) and Integrated Isotopic Ratio ($\delta^{18}O$, ‰) on the Ground as Well as the Properties of the First Peak in the Rainfall Rate (Intensity in mm hr^{-1}, the Integration Time at Which It Occurs in Minutes and the Instantaneous Isotopic Ratio in ‰)

				First rain peak		
Case	Description	Rain	$\delta^{18}O$	Intensity	Time	$\delta^{18}O$
A	All ice nucleation mechanisms active	15.32	−0.0	23.8	41.8	0.1
B	No ice nucleation mechanisms active	6.10	−4.4	113.5	39.6	−7.9
C	Only homogeneous ice nucleation active	4.90	−3.6	108.4	39.6	−7.9
D	Only heterogeneous ice nucleation active	17.08	0.1	23.8	41.8	0.1

depletes the atmospheric isotopic content during condensation, and thus, over time, the condensed phase isotopic ratio decreases. Second, the updraft transports the air parcel upward toward colder temperatures decreasing further the condensed phase isotopic ratio. However, this decrease of the in-cloud isotopic ratio due to the transport and depletion of heavy isotopologues is weaker than was predicted by the initial Rayleigh distillation profile (Figure 4), mainly because in the cloud, the relative humidity over water is always close to 100%. This leads to the strong difference in isotopic ratio between the early cirrus-like formation and the main cloud.

After the precipitation onset, the isotopic ratio decreases continuously above the melting level, under the influence of the large precipitating drops falling from the higher layers. This decrease is stronger at higher altitudes, where deposition takes place (above 7 km; Figure 1, right), with the isotopic ratio at the cloud top dropping to values as low as −43°. This evolution might well be an artifact due to the absence of relaxation between ice crystals and the environing air mass. This is underlined by the rapid increase of the isotopic ratio below the cloud where the melted drops exchange heavy isotopologues toward an equilibrium with the environment at 1 km of altitude, the relative humidity remains lower than 45% during the entire simulation. For example, at 6 km of altitude and after 31 min of integration time (where the first precipitation peak originates), all ice crystal sizes have an isotopic ratio of $-14 \pm 1.5°$. When the large precipitating crystals (larger than 200 μm) reach an altitude of 3.5 km, they have collected droplets from lower altitudes with higher isotopic ratios and therefore increase their isotopic ratio to $-11 \pm 1.5°$. As soon as the ice crystals melt, the droplets evaporate and most importantly exchange heavy isotopologues with the environing air mass. While large drops have a long characteristic relaxation time (at 0°C and saturation, τ_{drop}(500 μm drop) ~ 12 min), smaller drops (between 100 and 200 μm) reach quite rapidly the equilibrium (between 1 and 2 min at 0°C). Therefore, slightly below the melting level (2.5 km after 36.3 min of integration time), large drops ($r_d > 1$ mm) still have an isotopic ratio of $-10.7 \pm 1.7°$, but drops between 100 and 200 μm have an isotopic ratio of $-2.0 \pm 0.5°$). Finally, when the precipitation reaches the ground, the small drops have almost reached the equilibrium and have an isotopic ratio of $10.0 \pm 0.5°$ while the largest drops ($r_d \sim 4$ mm) show an isotopic ratio of −7.5°. The most populated drop sizes (between 1 and 2 mm) have an isotopic ratio between −1.3° and 1.7°.

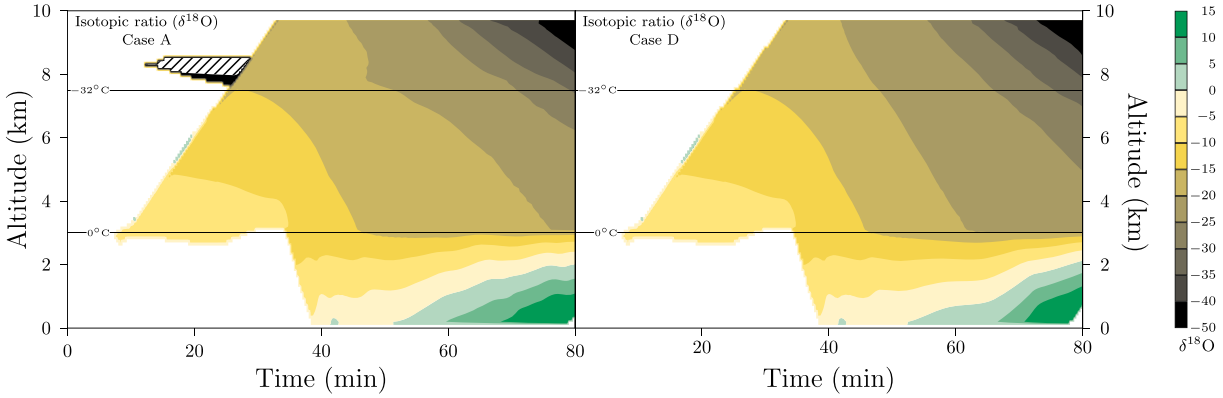

Figure 3. Oxygen-18 isotopic ratio in the condensed phase ($\delta^{18}O$, ‰) as a function of altitude and time simulated for (left) reference Case A where all ice nucleation mechanisms are taken into account and (right) sensitivity Case D where pristine ice is formed only through heterogeneous nucleation.

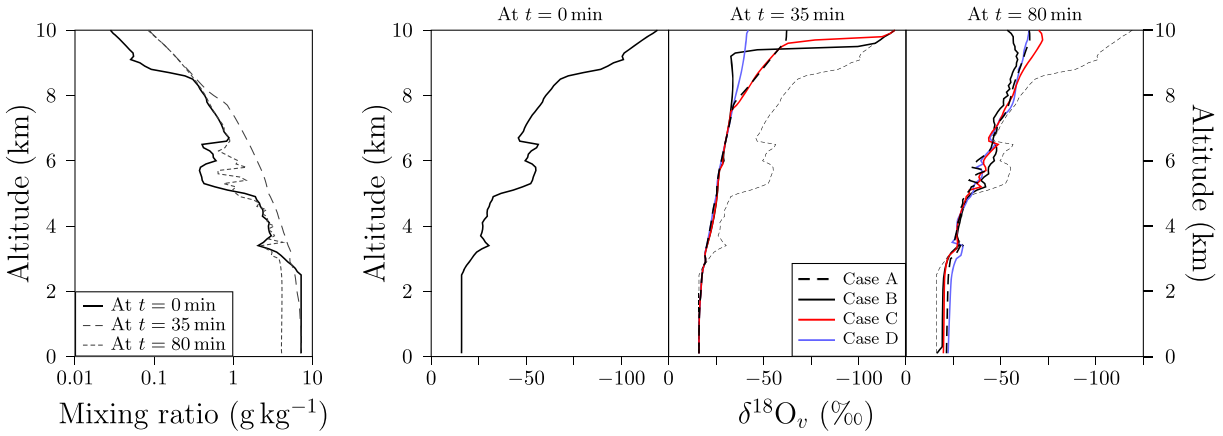

Figure 4. (Left) Mixing ratio profile of water vapor at the beginning of the simulation (from the sounding, Dye et al. (1986)—black thick continuous) and after 35 (thin short dashed) and 80 min of integration time (thin long dashed). (Right) Oxygen-18 isotopic ratio in the water vapor as a function of the altitude (right image, left panel) based on Rayleigh distillation at the beginning of the simulation (thin short dashed in the two next panels), (right image, center panel) after 35 min of integration time, at which point the cloud top reaches 9.7 km in reference Case A, for the case with all ice nucleation mechanisms (Case A, black dashed), with no ice nucleation mechanism (Case B, black continuous), with only homogeneous nucleation (Case C, red), and with only heterogeneous nucleation (Case D, blue), (right image, right panel) at the end of the simulation for all four cases.

The isotopic ratio in the instantaneous rainfall ($\delta^{18}O_A$; Figure 2, right) reflects this evolution, with an isotopic ratio at the first precipitation peak of $\delta^{18}O_A = 0.1°$, corresponding to the mean isotopic ratio of the most populated drop sizes. After the first peak of intensity, there is a small decrease of the isotopic ratio due to the increase in downdraft, which reduces the fall time of the droplets, leading to a lesser amplitude of the isotopic relaxation resulting in isotopic ratios ranging between −2% and 0‰. When the downdraft dies down (from 55 min of integration time on), the isotopic ratio in the rainfall gradually increases due to the combination of two factors: The mean drop radius decreases, and their residence time increases, and therefore, the rainfall isotopic ratio gets closer to the equilibrium with the air mass; even though the water vapor isotopic ratio at ground level slightly decreases (Figure 4), the relative humidity near the surface also decreases, from 28% at the first peak of intensity to 16% after 80 min of integration time, yielding a high pseudo-equilibrium isotopic ratio ($R_{l,\mathrm{eq}} = \alpha_{l,\mathrm{kin}} R_v$ with $\alpha_{l,\mathrm{kin}} > \alpha_{l,\mathrm{eq}}$ if $RH_w < 100\%$). The integrated value of the isotopic ratio in the precipitation for this reference case is $\delta^{18}O_A = -0.0°$ (Table 1).

3.2. Evolution of the ^{18}O Isotopic Ratio in the Water Vapor

The vertical profiles of the initial mixing ratio of water vapor and isotopic ratio in the water vapor for all four cases at three different times are presented in Figure 4.

The left panel in the right image of Figure 4 displays the original profile as computed by a Rayleigh distillation process (17). The profile appears to be quite irregular as a result of the asperities of the mixing ratio profile based on radiosoundings from Dye et al. (1986) used in Equation 17 (Figure 4, left). The constant isotopic ratio at low altitude is a result of the setting of absolute humidity as constant in the CCOPE dynamical case. The isotopic ratio then rapidly decreases with altitude along with the mixing ratio.

Once the cloud has developed, the decrease with altitude is much smaller, as the absolute humidity is close to saturation at all altitudes. Therefore, the profiles are closer to those usually used as original Rayleigh profiles (e.g., Bony et al., 2008, their Figure 6). All four considered cases display almost the same isotopic ratio below the homogeneous nucleation line (7.5 km). Above this altitude, the isotopic ratio for the cases where homogeneous ice nucleation is taken into account (Cases A and C), there is a strong depletion of ^{18}O isotopologues, whereas when only heterogeneous ice nucleation is taken into account (Case D), the decrease of the isotopic ratio occurs at the same rate as below 7.5 km.

This difference is a result of the condensation that is occurring above this altitude. When homogeneous nucleation is not taken into account, there is a relatively small amount of ice crystals that can consume water vapor, which results in quite strong supersaturations with respect to ice (at 9.5 km, $RH_i = 171\%$), and with respect to water ($RH_w = 108\%$). This supersaturation is in the same range as the supersaturation at lower altitudes, which is in good agreement with the continuous slope of the isotopic ratio. When homogeneous nucleation is taken into account, the number of ice crystals above 7.5 km increases strongly, leading to a

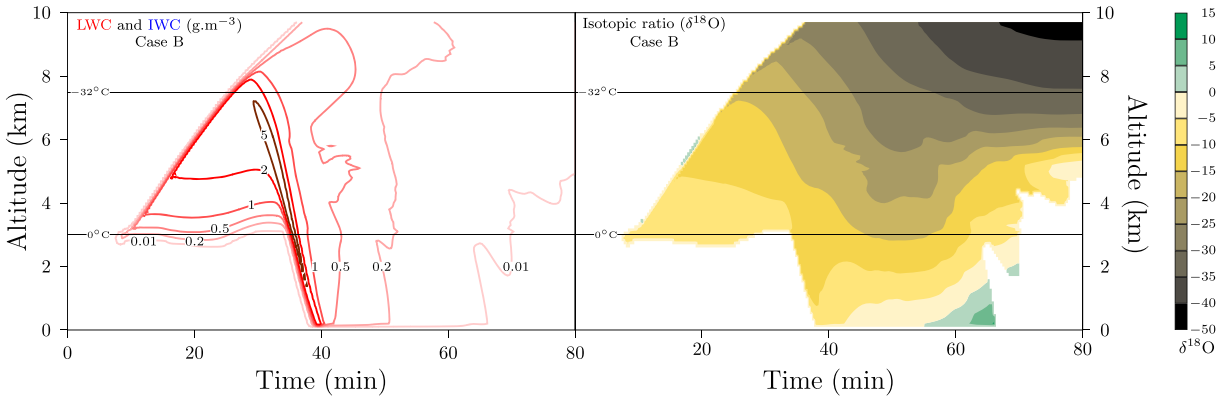

Figure 5. (Left) Liquid water content (g m^{-3}) and (right) oxygen-18 isotopic ratio in the condensed phase (δ^{18}O, ‰) as a function of altitude and time simulated for a case with no ice nucleation mechanism (Case B).

much larger consumption of water vapor. In return, the air mass becomes subsaturated with respect to water as the supersaturation with respect to ice strongly decreases ($RH_i = 116 \pm 2\%$ for Cases A and C). The difference in relative humidity with respect to ice impacts strongly the kinetic fractionation factor: At 8.5 km after 35 min, though all three cases have an equilibrium fractionation factor around 1.023, Cases A and C (where homogeneous nucleation is active) have a kinetic fractionation factor of 1.017 ± 0.001 while Case D (where homogeneous nucleation is inactive) has a kinetic fractionation factor of 1.007. This variation leads to the observed difference in the slope of the isotopic ratio in the water vapor from 7.5 to 9.5 km.

Finally, at the end of the simulation, mixing occurred between upper and lower layers of the atmosphere as well as with the surrounding air. Some slight differences are to be observed between the different cases, but overall, all four profiles are quite similar.

3.3. Sensitivity Studies Regarding the Microphysics

To investigate the impact of the different microphysical processes, three sensitivity studies are conducted: First, all ice nucleation mechanisms are suppressed (Case B), and then alternatively, only homogeneous nucleation (Case C) or only heterogeneous ice nucleation (Case D) is considered as the only pathway to pristine ice. The role of both ice nucleation mechanisms in the evolution of the cloud is then identified, and their impact on fractionation is discussed.

3.3.1. No Ice Nucleation Mechanisms: Case B

The first sensitivity case considers only liquid microphysics processes: All mechanisms from Equations 2 and 3 are taken into account except ice nucleation ($|_{\text{nucl}}$), riming ($|_{\text{rim}}$), and melting ($|_{\text{melt}}$). The liquid water content as a function of time and altitude is displayed in Figure 5, left. As for reference Case A, the cloud starts forming around 3 km altitude after 8.5 min of integration time. It reaches an altitude of 8.1 km only 22 min later, at which point the updraft has weakened and only a small quantity of water in the subsequent development reaches still higher altitudes. Precipitation is initiated between 7.1 and 7.7 km—altitudes close to the homogeneous nucleation line—after 28 min of cloud life time. The precipitation on the ground displays three distinctive regimes (black continuous curve in Figure 2, right): first a strong rainfall peak before decreasing rapidly. This high intensity is driven by high precipitating liquid water contents, despite small downdrafts. After 41.4 min of integration time the intensity increases slightly, corresponding to a maximum in the downward wind, resulting from the entrained air mass by the falling hydrometeors of the first peak in the rainfall rate. Finally, the downdraft dies down, and the precipitating water content decreases further (Figure 5, left), and the intensity of the precipitation weakens gradually. The cumulative precipitation for this Case B is of 6.10 mm (Table 1), a reduction of 60% with respect to Case A mostly due to the reduced downdraft after the first peak of intensity in the rainfall rate.

The evolution of the isotopic ratio in the liquid phase as a function of altitude and time is presented for ^{18}O isotopologues in Figure 5, right. When the cloud starts forming after 8 min, the same strong condensation rate as in Case A is observed. And as in Case A, the isotopic ratio decreases with increasing altitudes and time, with $\delta^{18}\text{O} \sim -6°$ at the cloud base and $\delta^{18}\text{O} \sim -26$ where the cloud top reaches 9.7 km. In contrast to reference Case A, this decrease with increasing altitude becomes steeper once the cloud top has reached the

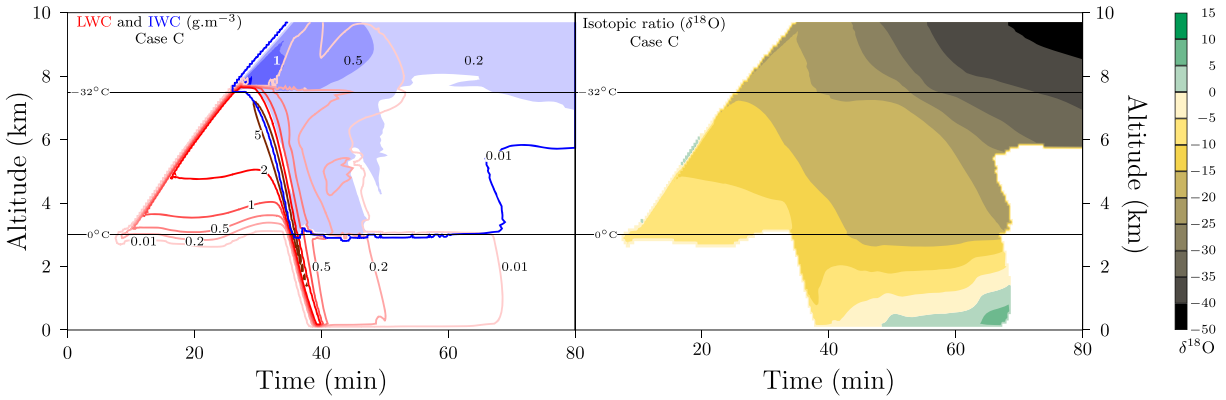

Figure 6. (Left) Liquid (red) and ice (blue) water contents (g m^{-3}) and (right) oxygen-18 isotopic ratio in the condensed phase (δ^{18}O, ‰) in the condensed phase as a function of altitude and time simulated for a case with pristine ice formed only through the homogeneous nucleation mechanism (Case C).

homogeneous nucleation line, as only smaller droplets with short characteristic relaxation times remain. Furthermore, the decrease of the isotopic ratio at lower altitudes after the precipitation onset is much stronger in this Case B than in Case A, as the amount of large precipitating drops falling from the higher layers is much larger (precipitating water content up to 300% higher). Particularly, as the precipitating drops are larger than in Case A (2.5 to 3.3 mm), their characteristic relaxation time is larger, and therefore, the condensate isotopic ratio in the precipitation is lower than in Case A, even though the equilibrium isotopic ratio is the same (in both cases, $\delta^{18}O_v = -16°$ and $RH_w = 28\%$)

In the early part of the precipitation, the instantaneous isotopic ratio of the surface precipitation is much lower than that of case A ($\delta^{18}O_B = -7.9°$ at the first precipitation peak—Figure 2, right). But this value then catches up with Case A and follows a quite similar evolution after 50 min of integration time, as the drop size gradually decreases, leading to an equilibrium with the air mass. As the downdraft dies down much earlier in Case B than in Case A, the humidity at the ground level increases back to its original value, and therefore, at the end of the simulation, $RH_w = 25\%$, resulting in a lower pseudo-equilibrium isotopic ratio. Overall, the mass-weighted, time-integrated value of the isotopic ratio in the precipitation for this sensitivity Case B is $\delta^{18}O_B = -4.4°$ (Table 1).

3.3.2. Only Homogeneous Ice Nucleation: Case C

The early development of the cloud is identical to Cases A and B, as it is not impacted by homogeneous nucleation; the dynamics is modified only when the cloud top reaches −32°C, due to the release of latent heat through ice formation and growth: The cloud top reaches 9.5 km after 34 min of integration time instead of 9.7 km in Case A and 9.1 km in Case B. The increase in updraft speed, with respect to sensitivity Case B, combined with the decreased volume of the precipitating drops due to the formation of ice crystals (Bergeron-Findeisen mechanism) yields a slight reduction of the rain intensity of the first peak (Figure 2, right) occurring after the same integration time as in Case B. Afterward, the downdraft is slightly delayed and reduced, which combined with a reduced precipitating liquid water content due to the smaller sedimentation speed of ice crystals leads to a decrease in the intensity of the second precipitation peak (Figure 2, right). The difference in vertical wind speeds is mostly caused by the reduced precipitating liquid water content, which limits the entrainment of the air mass. Given that only a small part of the ice crystals fall below melting temperatures, the consumption of latent heat due to the phase change is too small to impact significantly the dynamics below cloud. This results in a cumulative precipitation of 4.90 mm (Table 1).

The distribution of ^{18}O isotopologues in the domain in Case C is very similar to the distribution in Case B during the first 30 min of integration time (Figure 6, right). However, later, homogeneous nucleation impacts the evolution of the ^{18}O concentration: Above the homogeneous nucleation level, where the condensed phase almost solely consists of ice crystals, the isotopic ratio at first displays higher values than in Case B but then decreases faster as the larger ice crystals have fallen to lower altitudes.

Initially, in the in-cloud precipitating region, the isotopic ratio remains unchanged with respect to Case B: Precipitation starts at altitudes with temperatures above −32°C and only a small number of ice crystals contribute to the first peak of intensity. Shortly after this high precipitating water content has fallen, ice crystals become noticeable: At 3.5 km, slightly above the melting altitude, a small amount of ice crystals larger

than 2 mm contribute to the precipitation ($2 \cdot 10^{-6}$ cm^{-3}, 1 order of magnitude below the concentration of droplets with similar mass). Though their contribution to the total water content and to the total isotopic ratio is negligible, their microphysical impact is not. Their formation by freezing of large droplets above the homogeneous nucleation line leads to the evaporation in the downdraft of the remaining droplets through the Bergeron-Findeisen mechanism: At 3.5 km, the amount of droplets larger than 1.3 mm is reduced while the concentration of droplets smaller than 1.3 mm is increased. Furthermore, the isotopic ratio of the large droplets in Case C is larger than in Case B. This yields an increase in the isotopic ratio in the precipitation after 50 min of integration time. Two factors can be identified: on the one hand, the Bergeron-Findeisen mechanism which, due to droplet evaporation, increases the isotopic ratio in the droplets as their characteristic relaxation time reduces and, on the other hand, the larger relative proportion of large droplets which were formed at lower altitudes with higher isotopic ratios and never got transported through the updraft at altitudes above the homogeneous nucleation level. The resulting increase of the isotopic ratio in the rainfall is reflected also in the isotopic ratio of the cumulated precipitation: $\delta^{18}O_B = -3.6$ (Table 1).

3.3.3. Only Heterogeneous Ice Nucleation: Case D

Two essential mechanisms are taken into account for heterogeneous nucleation in Case D (Hiron & Flossmann, 2015): condensation freezing based on Meyers et al. (1992) and immersion freezing, adapted from Bigg (1953). Considering these mechanisms, the liquid and ice water contents evolve in a similar way to those of reference Case A. Combined, they lead to an efficient ice nucleation at relatively warm temperatures (the major part of the cloud is frozen before reaching the homogeneous nucleation line—Figure 1).

Due to the early onset of ice nucleation in the cloud development and the resulting latent heat release, the dynamics of the cloud is intensified with respect to sensitivity Case B (the cloud top reaches 9.7 km after 33.5 min of integration time). This increased updraft, combined with the dramatic change in the phase of the hydrometeors, leads to a delayed precipitation onset located at a lower altitude (between 5.5 and 6.5 km, same as in reference Case A). In addition, as the terminal velocities for ice crystals are smaller than for cloud droplets of identical mass, a large delay is noticed in the much smaller first peak of precipitations, similar to Case A (Figure 2, left). This decrease in intensity of the first peak results from the reduced total precipitating water content at precipitation onset. Here again, the second part of the precipitation on the ground (Figure 2, left) is marked by a dramatic increase in intensity because of the latent heat consumption at melting level. The cumulative precipitation amounts to 17.08 mm (Table 1), the largest of the four cases.

The contributions of homogeneous (Case C) and heterogeneous (Case D) ice nucleation show that in Case A, homogeneous ice nucleation does not significantly affect cloud dynamics, as most of the cloud is already frozen before reaching the homogeneous nucleation line. It increases the IWC in the cloud only above 8 km and reduces the late precipitating ice water content, leading to a slight reduction of the downdraft below the cloud after 60 min of simulation (reflected in the rainfall rate—Figure 2, left).

Figure 3 (right) displays the ^{18}O isotopic ratio as a function of time and altitude for Case D. The formation of the ice phase by heterogeneous nucleation has little impact on the isotopic ratio during the early cloud development as only a small amount of crystals are nucleated, but once the ice water content dominates in cloud, the condensed isotopic ratio takes a value of $\delta^{18}O_D = -18$ where the cloud top reaches 9.7 km, whereas, in Case B, $\delta^{18}O_B = -26$—Figures 3 (right) and 5 (right). This increase in the isotopic ratio is the result of large ice particles (radius larger than 200 μm) formed from rather large and consequently aged droplets, which have larger isotopic ratios than the smaller newly formed ice crystals.

In the precipitation region, an increase in the isotopic ratio with respect to Case B is observed, similar to Case C. Given the higher temperature of heterogeneous ice nucleation onset, the effects of the presence of ice crystals on the size of the hydrometeors and their isotopic ratio are increased. As the precipitating water drops form at lower altitudes than in Cases B and C, the isotopic ratio in the early phase of precipitation is higher: at 3.5 km, after 33 min of integration time, the isotopic ratio in the condensed phase has a value of −8.8°. This corresponds to relatively small drops (between 10 and 200 μm) grown mostly through vapor diffusion and collision coalescence at altitudes between 3 and 4 km and at equilibrium with the environing air mass. Once precipitating ice crystals reach 3.5 km after 35 min of integration time, the number of drops decreases, through the combination of riming and Bergeron-Findeisen process. As ice crystals reaching 3.5 km gradually originate from higher altitudes, their isotopic ratio gradually decreases. For the most abundant size of ice crystals (530 μm), the isotopic ratio is reduced from −12.8° after 38 min of integration time to −13.6° after 42 min. In the remainder of the precipitation system, the same mechanisms continue.

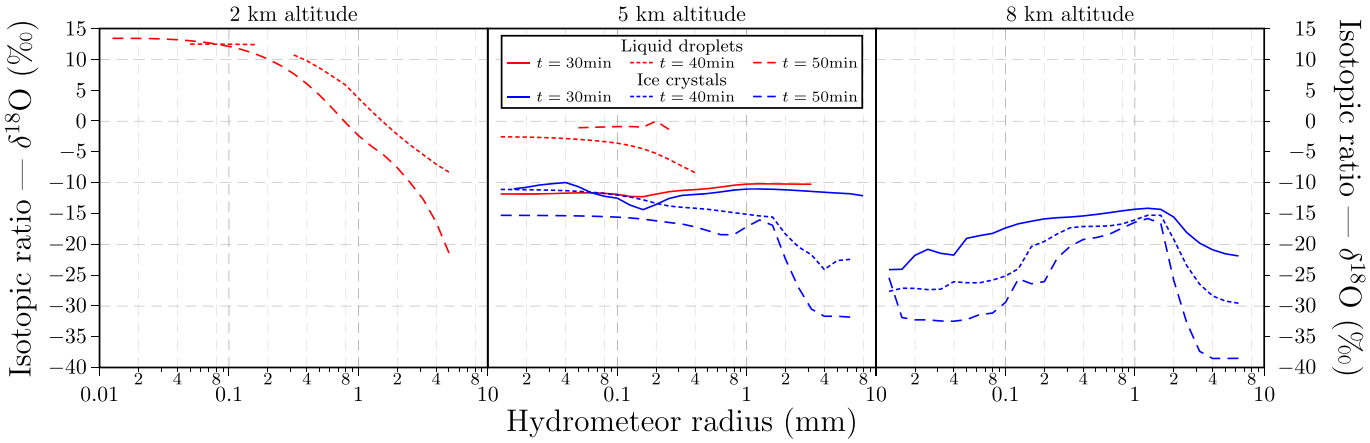

Figure 7. Isotopic ratio of water droplets (red) and ice crystals (blue) as a function of their radius for reference Case A, where all ice nucleation mechanisms are taken into account, after 30 (continuous), 40 (short dashed), and 50 (long dashed) min of integration time at 2 (left), 5 (center), and 8 (right) kilometers of altitude.

In contrast to reference Case A, in Case D, there is no competition between homogeneous and heterogeneous nucleation above 7.5 km of altitude. Therefore, in the late part of the precipitation, hydrometeors reach larger sizes as they grow mostly through vapor deposition at high altitudes (Figure 1, right), yielding an increase in the rainfall rate, and a smaller isotopic ratio in Case D than in the reference Case A, due to the increased characteristic relaxation time.

The isotopic ratio of the cumulated precipitation is also slightly reduced: $\delta^{18}O_D = 0.1°$ (Table 1).

3.3.4. Isotopic Ratio in the Hydrometeor Spectra

As most implementations of water isotopes in bulk microphysical parameterizations assume that the isotopic ratio is independent of particle size in a given hydrometeor category (e.g., rain), the ability of DESCAM to predict the isotopic ratio of each size particle independently is noteworthy. During the initial droplet formation, all droplets have the same isotopic ratio (Figure 7, center). Hydrometeors see their isotopic ratio continuously decrease during condensation due to the continuous impoverishment in ^{18}O of the ambient air mass, irrespective of their radius. This is due to the fact that during condensation, the relative humidity with respect to water keeps the same range (between 100% and 110%), yielding a steady impact on the kinetic fractionation factor (Figure 7, right).

However, once the hydrometeors reach a precipitating size, they fall rapidly toward altitudes with different water vapor isotopic ratios, temperatures, and relative humidity. These three factors combined lead to dramatic changes in the equilibrium condensed isotopic ratio. It is then that the characteristic relaxation time plays a major role. Large drops (radius larger than 1 mm) need more than 30 min at saturation and 30°C (temperature at ground level) to reach equilibrium with the environing air mass, while small droplets (radius smaller than 25 μm) need less than a second.

Figure 7 represents the isotopic ratio in the hydrometeor spectra for different altitudes at three time steps: after 30 min of integration time, in the updraft, shortly before the precipitation starts; after 40 min, during the first peak of rainfall intensity; and after 50 min, during the second peak of rainfall intensity. The water drops spectra below cloud show the importance of the relaxation time in the isotopic ratio: Droplets with radii smaller than 100 to 200 μm have an isotopic ratio in a small range, corresponding to the equilibrium condensed isotopic ratio, while the isotopic ratio strongly decreases with increasing radius for larger drops with values coming close to those of large ice crystals at 5 km of altitude.

In the middle panel (5 km of altitude), after 30 min of integration time, the isotopic ratios of ice crystals and cloud drops are very close as most ice crystals are freshly formed through heterogeneous nucleation. After 40 min, the isotopic ratio of small ice crystals remains in the same range whereas the isotopic ratio of cloud droplets increases as the relative humidity with respect to water drops below 100%. Here also, the effect of the relaxation characteristic time can be noticed for droplets larger than 100 μm.

The difference in behavior between large and small drops is also illustrated by the mean isotopic ratio for different periods during precipitation presented in Figure 8. All spectra display an increase of the isotopic

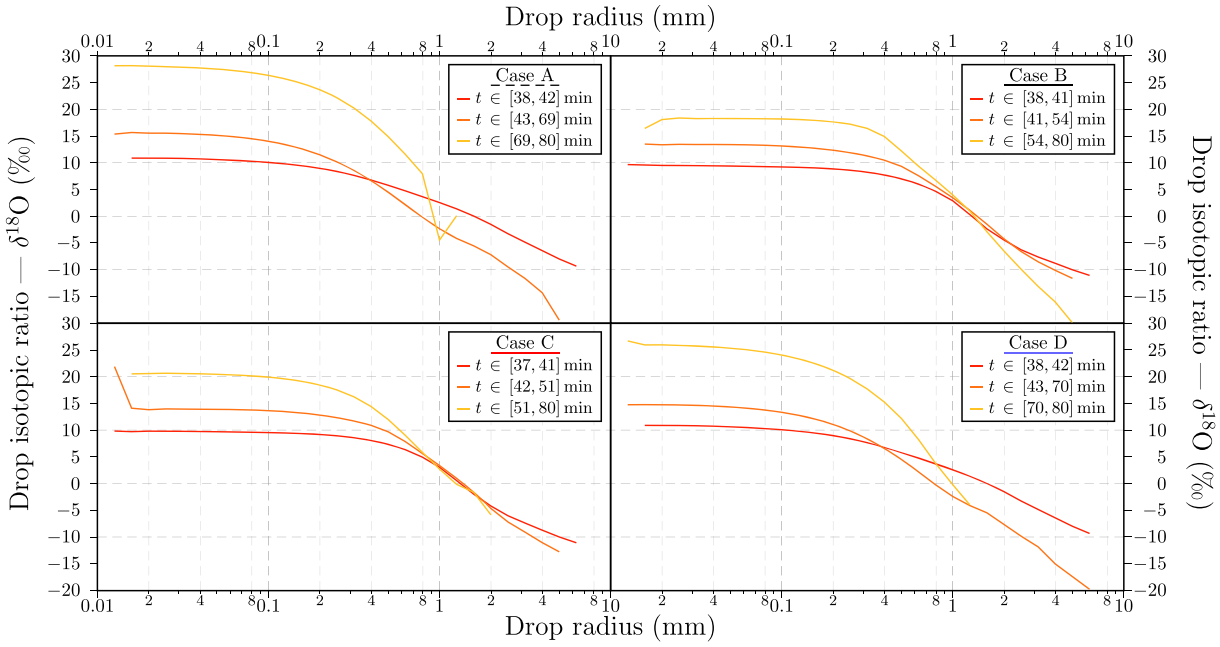

Figure 8. Mean isotopic ratio in the rain on the ground as a function of the drop radius in the first peak of intensity (red), in the downdraft-driven second peak of intensity (orange) and in the remainder of the precipitation (yellow) for all four cases: reference Case A where all ice nucleation mechanisms are taken into account (top left), Case B where no ice nucleation mechanism is taken into account (top right), Case C where only homogeneous ice nucleation is taken into account (bottom left), and Case D where only heterogeneous ice nucleation is taken into account (bottom right).

ratio with decreasing radii toward a plateau corresponding to the equilibrium with the environing air mass for drops smaller than 0.2 mm. This decrease is in good agreement with the modeling results of Lee and Fung (2008).

All four cases display very similar isotopic ratios in the first peak of intensity with the largest drops presenting an isotopic ratio around −10° and a plateau close to 10°. However, there is a difference of 3° for drops between 2 and 4,mm which results in the difference in value at the first peak of intensity previously noted. This fact can mostly be attributed to the origin of the precipitation: The large drops in Cases A and D originate from lower altitudes than in Cases B and C and therefore display a higher isotopic ratio. Given their large size, the impact of the relaxation toward equilibrium is fairly limited.

In the second peak of intensity, driven by the downdraft, the large drops in Cases A and D have a lower isotopic ratio than in the first peak of intensity. This is the result of two combined factors: in part because the drops mostly originate from higher altitudes with slightly lower isotopic ratios, but most importantly because the strong downdraft (up to 10 m s^{-1}) reduce the residence time in subsaturated areas, limiting further the effect of the relaxation toward equilibrium.

Finally, in the remainder of the precipitation, only small drops still reach the ground as the downdraft has died down and the relative humidity remains low at ground level (between 15% and 25%) leading to a large evaporation of the precipitating drops. This causes a high isotopic ratio in the "plateau" (∼27 for Cases A and D and ∼20 for Cases B and C) and therefore a high isotopic ratio in the rainfall.

3.4. Sensitivity Studies Regarding the Fractionation Calculation

Though there seems to be a signature for the different microphysics cases (lower values for the case with only liquid processes and higher values for cases with heterogeneous ice nucleation and intermediate values for the case with only homogeneous ice nucleation), the origin of the signature is ambiguous: The isotopic ratio in ground precipitation seems to be a result of the microphysical feedback on the dynamics, but it can also be a result of the difference between fractionation on droplets and ice crystals. Some technical choices can also play a role in our results: What are the impacts of the absence of fractionation during sublimation, as well as the relaxation toward equilibrium of heavy isotopologues in ice crystals? These aspects are studied in the following sections.

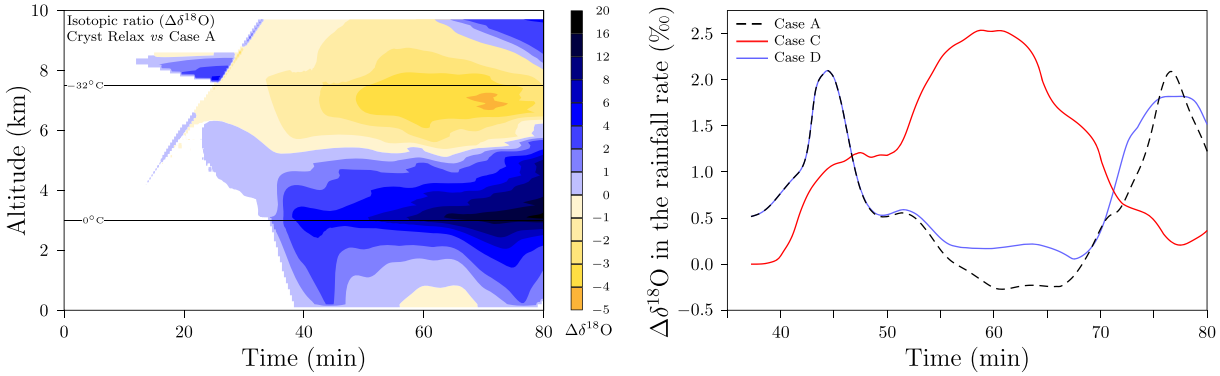

Figure 9. (Left) Deviation in isotopic ratio in the condensed phase as a function of altitude and time between the reference cases and the sensitivity cases ($\Delta\delta^{18}O = \delta^{18}O_{sens} - \delta^{18}O_{ref}$) where isotopologues in ice crystals are computed using the relaxation scheme presented in Equation 12 for water droplets ($\delta^{18}O_{sens}$) and the corresponding reference case ($\delta^{18}O_{ref}$), for the Case A where all ice nucleation mechanisms are taken into account, and (right) deviation in isotopic ratio in the precipitation as a function of time for Cases A (all ice nucleation processes, black), C (only homogeneous nucleation, red), and D (only heterogeneous nucleation, blue).

To test the different modifications, the relaxation of heavy isotopologues in ice crystals needs to be taken into account first. Indeed, to compare the impact of the fractionation factor difference between both phases or the impact of the equilibrium assumption, ice crystals and liquid drops need to behave in a similar manner. This second sensitivity study will be expressed in terms of variation with respect to the simulation with ice crystal relaxation.

3.4.1. Full Fractionation Calculation for Ice Crystals

In the previous sections, it was assumed that no isotopic fractionation occurred during the sublimation of ice crystals and that the isotopic relaxation phenomenon did not occur. This assumption, combined with the assumption of the homogeneity of the isotopic ratio in the ice crystal, might however introduce some error in the calculation of the hydrometeor isotopic ratio.

A sensitivity study is performed in which the isotopic ratio in ice crystals evolves following the adaptation to ice of Equation 12 in order to get an estimate on the potential impact of such an effect. The evolution of the ^{18}O isotopic ratio as a function of altitude and time is presented in Figure 9 (left) for Case A, where all ice nucleation mechanisms are taken into account. The early evolution of the isotopic ratio in the cloud (until 30 min of integration time) is identical to the reference case (Figure 3, left) with the exception of the early cirrus-like formation. This is to be expected as during this period, the formed ice crystals are of a rather small size, with the exception of those in the cirrus-like formation, and therefore are always at equilibrium. Furthermore, as was pointed out earlier, in-cloud ice crystals grow rather rapidly because of the strong dynamics and high relative humidity in the cloud, and therefore, the last formed shell of the ice crystal is at equilibrium with the environing air mass. Once ice crystals reach a larger size through either depositional growth or riming and subsequently fall as they reach a sedimentation size, the relaxation starts having an effect on the condensed phase isotopic ratio. The evolution of the isotopic ratio is then rather similar to what was observed for Case B where only the liquid phase was considered: For example, between 3 and 5.5 km, for a given altitude, due to the relaxation of the ice crsystals toward equilibrium with the environing air mass, the isotopic ratio remains relatively constant before gradually increasing, whereas it steadily decreased in the reference case as the ice crystals came from higher altitudes with lower isotopic ratios which were kept constant during sublimation. The maximum difference between the reference case and the sensitivity case is to be noticed, for all times, around the melting altitude: As relaxation is taken into account for ice crystals, their isotopic ratio in the lower altitudes of the cloud is noticeably higher than in the reference case, but once the hydrometeors melt, they relax toward isotopic ratios very close to those of the reference case, hence the decrease in difference below the cloud.

The resulting variation of the isotopic ratio in the rainfall for Cases A, C, and D is presented in Figure 9, right. As soon as the precipitation starts, the relaxation of ice crystals has an effect on the isotopic ratio in Cases A and D. The increase of the isotopic ratio in the first peak of intensity (up to 2‰ at the peak) is the result of an earlier relaxation of the hydrometeors than in the reference cases, which is not compensated by the water drops relaxation below cloud because of their large size and therefore long characteristic relaxation

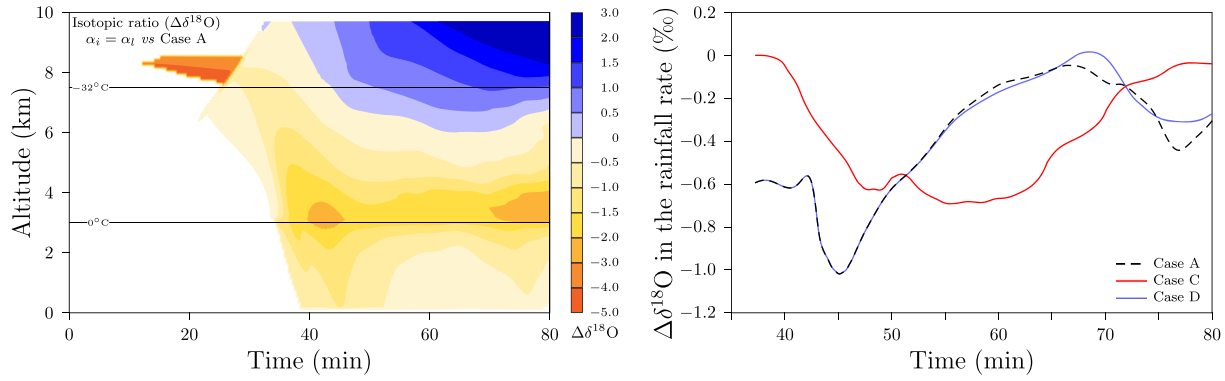

Figure 10. Difference in isotopic ratio between the reference cases and the sensitivity cases considering $\alpha_{i,\mathrm{kin}} = \alpha_{l,\mathrm{kin}}$: $\Delta\delta^{18}\mathrm{O} = \delta^{18}\mathrm{O}_{\mathrm{sens}} - \delta^{18}\mathrm{O}_{\mathrm{ref}}$. (Left) In the condensed phase as a function of altitude and time for Case A, where all ice nucleation mechanisms are taken into account, and (right) in the precipitation as a function of time for Cases A (all ice nucleation processes, black), C (only homogeneous nucleation, red), and D (only heterogeneous nucleation, blue).

time. The differences then decrease once the precipitation becomes driven by the downdraft. In this part of the precipitation, smaller hydrometeors contribute to the precipitation with shorter characteristic relaxation times, bringing their isotopic ratio closer to equilibrium than in the first peak of intensity. The decrease of the isotopic ratio in the precipitation is therefore a direct effect of the reduced water vapor isotopic ratio: Ice crystals relax toward a higher isotopic ratio than water droplets, and by doing so, they consume more heavy isotopologues than water droplets do. As a result, the water vapor isotopic ratio rapidly drops in the downdraft for altitudes below about 5.5 km. The liquid nature of the first peak of intensity in Case C is confirmed by the absence of variation in the isotopic ratio between the present simulation and the reference case. However, once ice crystals contribute to the precipitation, the difference increases up to 2.5‰.

Though the variation introduced by the consideration of ice crystals relaxation seems quite minor with respect to the total variation of the isotopic ratio during the precipitation (about 10%), it occurs in Cases A and D when the rainfall rate is at its maximum. It therefore yields a noticeable difference in the accumulated isotopic ratio: $\Delta\delta^{18}\mathrm{O}_A = 0.9\%0$, $\Delta\delta^{18}\mathrm{O}_C = 0.8$, and $\Delta\delta^{18}\mathrm{O}_D = 0.9$, but it does not really impact the isotopic signature of the different cases in these dynamics. This might however not be true in calmer dynamics where the relaxation of ice crystals could become more important in the cloud.

3.4.2. Microphysics Versus Fractionation

To test the importance of the difference in fractionation factors between the ice and liquid phase, the following sensitivity test is considered: All fractionation is computed using only the liquid phase fractionation factors, yielding $\alpha_{i,\mathrm{kin}} = \alpha_{l,\mathrm{kin}}$. The results are presented in terms of differences in the isotopic ratio with respect to the reference cases (corresponding to the Cases A, C, and D presented in section 3.4.1).

Figure 10 (left) presents the evolution of the difference between the sensitivity case and the reference case as a function of altitude and time for Case A where all ice nucleation mechanisms are taken into account. In the early cirrus-like formation, the decrease in fractionation factor leads to a decrease of the condensed isotopic ratio. As the relative humidity with respect to ice is close to 100%, the difference in condensed isotopic ratio is proportional to $\alpha_{l,\mathrm{kin}} - \alpha_{i,\mathrm{kin}}$.

In the early development of the cloud and until hydrometeors reach their sedimentation radius, the impact of the modification of the fractionation factor is fairly limited. However, once hydrometeors fall, they reach altitudes where they are out of equilibrium. Given that the characteristic relaxation time is proportional to the fractionation factor (see Equation 13), the precipitating ice crystals reach equilibrium faster than in the reference case, but the equilibrium in question corresponds to a lower isotopic ratio as it is defined as $R_{i,\mathrm{eq}} = \alpha_{l,\mathrm{kin}} \cdot R_v$. This leads to a decrease in the isotopic ratio of the condensed phase. When ice crystals melt, the hydrometeors resume to their original behavior, and therefore, the isotopic ratio above 0°C increases back toward the values from the reference case.

A different mechanism occurs at high altitude: The formed ice crystals rarely reach sedimenting radii and therefore have long residence times. Given the relatively high ice water content at these altitudes, the continuous deposition of water vapor consumes heavy isotopologues, resulting in a depletion. As the fractionation

factor is reduced in the sensitivity case, the depletion of the water vapor is limited, and therefore, the isotopic ratio in the condensed phase (as well as in the water vapor) is increased at high altitudes.

Figure 10 (right) presents the evolution of the variation of the isotopic ratio in the surface precipitation. In this series of simulations, the longer the residence time of the ice crystals, the lower the isotopic ratio. Remarks similar to those for the previous section can be done for the first peak of intensity in Case C as well as the implication of the increased downdraft in Cases A and D. The impact on the accumulated isotopic ratio is here again noticeable: $\Delta\delta^{18}O_A = -0.7$, $\Delta\delta^{18}O_C = -0.3$, and $\Delta\delta^{18}O_D = -0.6$

4. Conclusions

Isotopic fractionation of water is a fundamental tool used to infer past climate variations. The present study is one of the first to use bin microphysics while investigating the potential influence of cloud-scale effects on the fractionation.

In a first attempt, a 1.5D dynamic framework was coupled to the bin-resolved microphysics module DESCAM (Flossmann & Wobrock, 2010) to limit the study to a small-scale convective cloud. A size-resolved treatment of the isotopic fraction of water vapor and condensed liquid water and ice was added to follow in detail the fractionation process through cloud and precipitation evolution.

A second study was dedicated to the microphysical state of the cloud when liquid and ice pathways were varied. Here, variations of the isotopic ratio up to a value of 8° could be found in the precipitation on the ground. However, a careful analysis showed that the modification was essentially due to the resulting change in the importance of phase transitions. The effects only due to a modified liquid/ice fractionation coefficient were more modest, on the order of 1 per mil. More importantly, as soon as the rainfall rate decreased below 25 mm hr^{-1}, particularly when constituted of small hydrometeors, the precipitation isotopic ratio was mostly driven by a combination of the relative humidity and water vapor isotopic ratio at low levels.

Thus, it seems not possible to read the pathway of precipitation formation from the isotopic fraction in the rain water. In this, the granulometry of the precipitation observations in time is particularly important for the analysis of the measured isotopic ratio. However, the strong convective nature of the modeled cloud as well as its relatively high cloud base and the low relative humidity at the ground is not representative of all precipitating clouds.

The current study is very preliminary, as the very first of its kind. In a further step, the dynamical framework of the model needs to be replaced with a more complex 3D mesoscale dynamics. Then, the effect of more stratiform clouds and longer lasting phase change periods on the evolution of the fractionation in the cloud and the precipitation can be investigated in more detail to check whether information on the phase changes could be traced and identified in the precipitations under certain conditions. Also, in a larger 3D scale, the effects of transport of isotopic ratios with respect to local phase changes can be addressed. Finally, the prediction and validation of deuterium excess signals in hydrometeors and precipitation can be addressed.

Data Availability Statement

The data produced in this modeling study are available at Hiron and Flossmann (2019). A detailed description of the model can be found in Flossmann and Wobrock (2010).

Acknowledgments
This research was funded by Project AC-AHC^2 Grant Number ANR-15-CE01-0015 of the French National Agency of Research ANR. The authors acknowledge with gratitude the support provided. Two anonymous reviewers are thanked for their suggestions and thorough remarks, which greatly benefited this manuscript.

References

Asai, T., & Kasahara, A. (1967). A theoretical study of the compensating downward motions associated with cumulus clouds. *Journal of the Atmospheric Sciences*, *24*(5), 487–496. https://doi.org/10.1175/1520-0469(1967)024<0487:atsotc>2.0.co;2

Bigg, E. K. (1953). The formation of atmospheric ice crystals by the freezing of droplets. *Quarterly Journal of the Royal Meteorological Society*, *79*(342), 510–519. https://doi.org/10.1002/qj.49707934207

Bolot, M., Legras, B., & Moyer, E. J. (2013). Modelling and interpreting the isotopic composition of water vapour in convective updrafts. *Atmospheric Chemistry and Physics*, *13*, 7903–7935. https://doi.org/10.5194/acp-13-7903-2013

Bony, S., Risi, C., & Vimeux, F. (2008). Influence of convective processes on the isotopic composition (δ^{18}O and δd) of precipitation and water vapor in the tropics: 1. Radiative-convective equilibrium and tropical Ocean-Global Atmosphere-Coupled Ocean-Atmosphere response experiment (TOGA-COARE) simulations. *Journal of Geophysical Research*, *113*, D19306. https://doi.org/10.1029/2008JD009943

Dansgaard, W. (1964). Stable isotopes in precipitation. *Tellus*, *16*(4), 436–468.

Dye, J., Jones, J., Winn, W., Cerni, T., Gardiner, B., Lamb, D., et al. (1986). Early electrification and precipitation development in a small, isolated Montana Cumulonimbus. *Journal of Geophysical Research*, *91*(D1), 1231–1247. https://doi.org/10.1029/JD091id01p01231

Ehhalt, D. H. (1974). Vertical profiles of HTO, HDO, and H_2O in the troposphere: Atmospheric Quality and Modification Division, National Center. https://doi.org/10.5065/D6BP00QB

Flossmann, A. I., Hall, W., & Pruppacher, H. R. (1985). Theoretical study of the wet removal of atmospheric pollutants. Part I: The redistribution of aerosol particles captured through nucleation and impaction scavenging by growing cloud drops. *Journal of the Atmospheric Sciences*, *42*(6), 583–606. https://doi.org/10.1175/1520-0469(1985)042<0583:atsotw>2.0.co;2

Flossmann, A. I., & Wobrock, W. (2010). A review of our understanding of the aerosol-cloud interaction from the perspective of a bin resolved cloud scale modelling. *Atmospheric Research*, *97*(4), 478–497. https://doi.org/10.1016/j.atmosres.2010.05.008

Gonfiantini, R. (1978). Standards for stable isotope measurements in natural compounds. *Nature*, *271*(5645), 534–536. https://doi.org/10.1038/271534a0

Hays, P. D., & Grossman, E. L. (1991). Oxygen isotopes in meteoric calcite cements as indicators of continental paleoclimate. *Geology*, *19*(5), 441–444.

Herbert, R. J., Murray, B. J., Dobbie, S. J., & Koop, T. (2015). Sensitivity of liquid clouds to homogenous freezing parameterizations. *Geophysical Research Letters*, *42*, 1599–1605. https://doi.org/10.1002/2014GL062729

Hiron, T., & Flossmann, A. I. (2015). A study of the role of the parameterization of heterogeneous ice nucleation for the modeling of microphysics and precipitation of a convective cloud. *Journal of the Atmospheric Sciences*, *72*(9), 3322–3339. https://doi.org/10.1175/jas-d-15-0026.1

Hiron, T., & Flossmann, A. I. (2019). Dataset dataset for "atmospheric oxygen isotopic fractionation in clouds: A bin resolved microphysics model approach". https://doi.org/10.5281/zenodo.4001917

Jaenicke, R. (1988). Aerosol physics and chemistry. In G. Fischer (Ed.), *Numerical Data and Functional Relationships in Science and Technology* (Vol. 4b, pp. 391–457).

Joussaume, S., & Jouzel, J. (1993). Paleoclimatic tracers: An investigation using an atmospheric general circulation model under ice age conditions: 2. water isotopes. *Journal of Geophysical Research*, *98*(D2), 2807–2830. https://doi.org/10.1029/92JD01920

Jouzel, J., & Merlivat, L. (1984). Deuterium and oxygen 18 in precipitation: Modeling of the isotopic effects during snow formation. *Journal of Geophysical Research*, *89*(D7), 11,749–11,757.

Koop, T., Luo, B., Tsias, A., & Peter, T. (2000). Water activity as the determinant for homogeneous ice nucleation in aqueous solutions. *Nature*, *406*(6796), 611–614. https://doi.org/10.1038/35020537

Lee, J.-E., & Fung, I. (2008). "Amount effect" of water isotopes and quantitative analysis of post-condensation processes. *Hydrological Processes*, *22*(1), 1–8. https://doi.org/10.1002/hyp.6637

Leroy, D., Monier, M., Wobrock, W., & Flossmann, A. I. (2006). A numerical study of the effects of the aerosol particle spectrum on the development of the ice phase and precipitation formation. *Atmospheric Research*, *80*(1), 15–45. https://doi.org/10.1016/j.atmosres.2005.06.007

Majoube, M. (1970). Fractionation factor of ^{18}O between water vapour and ice. *Nature*, *226*, 1242. https://doi.org/10.1038/2261242a0

Majoube, M. (1971). Fractionnement en oxygène 18 et en deutérium entre l'eau et sa vapeur. *Journal de Chimie Physique*, *68*, 1423–1436. https://doi.org/10.1051/jcp/1971681423

Merlivat, L., & Nief, G. (1967). Fractionnement isotopique lors des changements d état solide-vapeur et liquide-vapeur de l'eau à des températures inférieures à 0 c. *Tellus*, *19*(1), 122–127.

Meyers, M. P., DeMott, P. J., & Cotton, W. R. (1992). New primary ice-nucleation parametrizations in an explicit cloud model. *Journal of Applied Meteorology*, *31*, 708–721. https://doi.org/10.1175/1520-0450(1992)031<0708:npinpi>2.0.co;2

Moore, M., Blossey, P. N., Muhlbauer, A., & Kuang, Z. (2016). Microphysical controls on the isotopic composition of wintertime orographic precipitation. *Journal of Geophysical Research: Atmospheres*, *121*, 7235–7253. https://doi.org/10.1002/2015JD023763

Petters, M. D., & Kreidenweis, S. M. (2007). A single parameter representation of hygroscopic growth and cloud condensation nucleus activity. *Atmospheric Chemistry and Physics*, *7*(8), 1961–1971. https://doi.org/10.5194/acp-7-1961-2007